

Measurement of Ampère-class pulsed electron beams via field emission from carbon-nanotube cathodes in a radiofrequency gun

D. Mihalcea, L. Faillace, J. Hartzell, H. Panuganti, S. Boucher, A. Murokh, P. Piot, and J. C. T. Thangaraj

Citation: [Applied Physics Letters](#) **107**, 033502 (2015); doi: 10.1063/1.4927052

View online: <http://dx.doi.org/10.1063/1.4927052>

View Table of Contents: <http://scitation.aip.org/content/aip/journal/apl/107/3?ver=pdfcov>

Published by the [AIP Publishing](#)

Articles you may be interested in

[CTR Bunch Length Measurement of Monoenergetic and Maxwellian Electron Beams from Laser Plasma Cathode](#)

AIP Conf. Proc. **877**, 799 (2006); 10.1063/1.2409218

[Integrally gated carbon nanotube field emission cathodes produced by standard microfabrication techniques](#)

J. Vac. Sci. Technol. B **21**, 957 (2003); 10.1116/1.1565343

[Fabrication and electrical characteristics of carbon nanotube-based microcathodes for use in a parallel electron-beam lithography system](#)

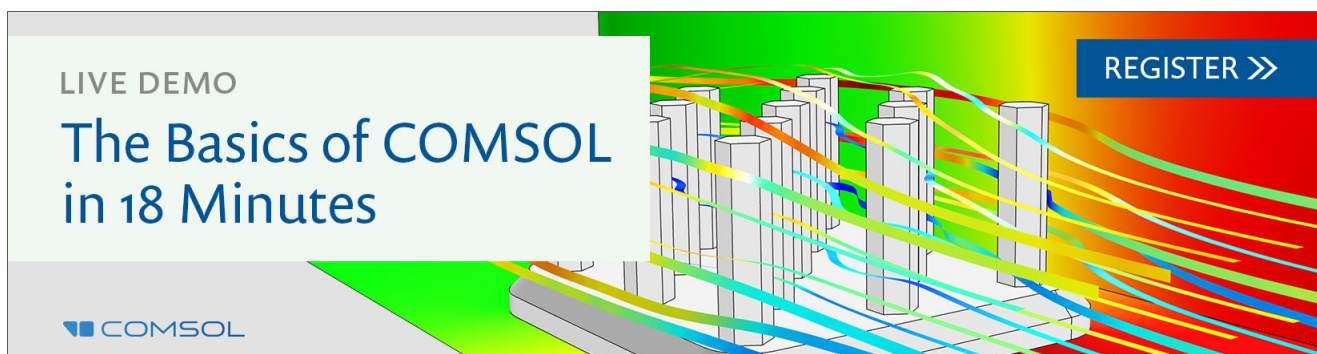
J. Vac. Sci. Technol. B **21**, 693 (2003); 10.1116/1.1545755

[The Study of Explosive Emission from Carbon Nanotubes](#)

AIP Conf. Proc. **650**, 385 (2002); 10.1063/1.1530879

[Field emission from carbon nanotubes and its application to electron sources](#)

AIP Conf. Proc. **486**, 439 (1999); 10.1063/1.59826

A promotional banner for a COMSOL live demo. The background features a 3D model of a multi-column structure with colorful streamlines representing flow or field lines. The text 'LIVE DEMO' is in the top left, 'The Basics of COMSOL in 18 Minutes' is in the center, and 'REGISTER >>' is in a blue button in the top right. The COMSOL logo is in the bottom left.

LIVE DEMO

The Basics of COMSOL in 18 Minutes

REGISTER >>

COMSOL

Measurement of Ampère-class pulsed electron beams via field emission from carbon-nanotube cathodes in a radiofrequency gun

D. Mihalcea,¹ L. Faillace,² J. Hartzell,² H. Panuganti,¹ S. Boucher,² A. Murokh,² P. Piot,^{1,3} and J. C. T. Thangaraj³

¹Northern Illinois Center for Accelerator and Detector Development and Department of Physics, Northern Illinois University, DeKalb, Illinois 60115, USA

²RadiaBeam Technologies LLC, Santa Monica, California 90404, USA

³Fermi National Accelerator Laboratory, Batavia, Illinois 60510, USA

(Received 10 February 2015; accepted 8 July 2015; published online 20 July 2015)

Pulsed field emission from cold carbon-nanotube cathodes placed in a radiofrequency resonant cavity was directly measured. The cathodes were located on the backplate of a conventional $1 + \frac{1}{2}$ -cell resonant cavity operating at 1.3-GHz and resulted in the production of bunch train with maximum average current close to 0.7 Ampère. The measured Fowler-Nordheim characteristic, transverse emittance, and pulse duration are presented and, when possible, compared to numerical simulations. The implications of our results to the promise of high-average-current electron sources are briefly discussed. © 2015 AIP Publishing LLC. [<http://dx.doi.org/10.1063/1.4927052>]

Over the last decades, field-emission (FE)—the emission of electrons via tunneling effect—has led to the development of compact electron sources that have been widely disseminated in microelectronics,¹ electron microscopy,² and more recently as particle-accelerator sources.³ FE enjoys a greater simplicity compared to other types of electron-emission mechanisms: it does not require auxiliary systems such as lasers employed in photoemission nor needs to be electrically heated by a filament as for thermionic cathode. A FE cathode operates with intense [$\mathcal{O}(\text{GV}/\text{m})$] electric fields applied at its surface. The field bends the potential barrier of the material and enhances the probability for electron tunneling. In practice, given the limited electric-field amplitude sustainable in common apparatus (10–100 MV/m), the generation of large field relies on field enhancement provided by sharp microscopic features present at the surface of the FE cathode. Such attribute results in the local field in the vicinity of the features $E_e = \beta_e E$, where β_e is the enhancement factor and E is the applied (macroscopic) field. Consequently, the current density emitted from one of the sharp features is governed by the Fowler-Nordheim's (FN's) law⁴ $j = aE_e^2 \exp\left(\frac{b}{E_e}\right) \hat{n}$, where $a \equiv \frac{1.42 \times 10^{-6}}{\Phi} \exp\left(\frac{10.4}{\Phi^{1/2}}\right)$ and $b \equiv -6.56 \times 10^9 \Phi^{3/2}$ are constants that depend on the material work function Φ (in units of eV),⁵ \hat{n} is the unitary vector normal to the local emitting surface. FE cathodes consisting of single field emitter have been proposed as source of ultra-bright electron bunches.⁶ Conversely, FE cathodes composed of a large number of field emitters are contemplated as high-current electron sources that could be deployed in a variety of contexts ranging from fundamental science along with medical, industrial, and security settings. Finally, the application of a time-dependent electric field results in the generation of electron bunches with finite duration.^{7–10} CNTs are allotropes of carbon with a cylindrical nanostructure and with exceptional electrical and mechanical properties. CNTs are fibers with diameters ranging from 1 to 50 nm, coming in either single-wall or multi-wall strands and with large aspect

ratios.¹¹ These properties yield substantial field enhancement factors, and—alongside with their low electrical resistance, high thermal stability, and robustness to high temperatures—CNTs are excellent candidates for FE cathodes. CNTs can be synthesized as aligned field-emitter arrays (FEA) or configured as randomly oriented field emitters deposited on surfaces. Although FEAs are ideal for most applications, especially in vacuum microelectronics¹² and are generally produced via chemical vapor deposition (CVD)¹³ randomly distributed CNTs can be produced with simpler, fast, and inexpensive fabrication process known as electrophoretic deposition (EPD) which can easily be applied to large surfaces non-planar.¹⁴

In this letter, we report on the experimental demonstration of stable pulsed emission from CNT cathodes with currents at the Ampère level. The achieved parameters could permit direct injection in a radiofrequency (RF) linear accelerator for acceleration to MeV energies thereby producing MW average beam powers. Such high-average power electron beams have application to high-power accelerator-based light sources,¹⁵ electron cooling to increase the luminosity of high energy of ion-beam colliders,¹⁶ as well as a possibility of introducing accelerator driven nuclear waste management and transmutation facilities. Additionally, the ionizing radiation produced by MW electron beams could be used to modify the physical, chemical, or biological properties of materials¹⁷ in high-throughput industrial facilities.

The cathodes used in our experiments were synthesized using an EPD process and consisted of a layer of multiple allotropes of carbon including nanotubes, buckyballs, graphite, and amorphous carbon,¹⁸ see Fig. 1(a). Emerging from this layer are a vast number of randomly oriented nanotubes. The tubes have an average length of $\sim 3 \mu\text{m}$ with a diameter of a few nanometers. The film thickness used for our cathodes is a few microns. There is an interlayer between the CNT deposition and the substrate that is a mixture of conducting and dielectric material. The current formed by such cathodes is $I \simeq \mathcal{A}j$, where \mathcal{A} is the effective emission area. Two

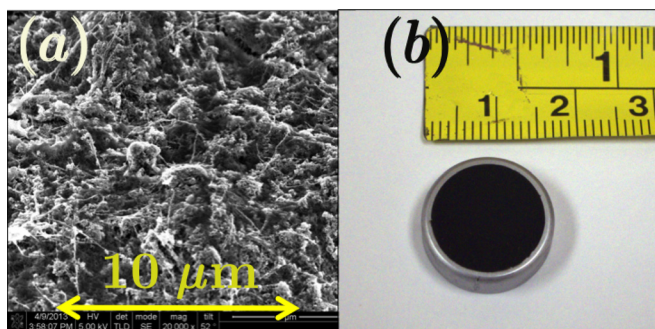


FIG. 1. Micrograph of CNT cathode surface (a) and photograph of the CNT cathode on its molybdenum substrate (b).

cathodes were tested, a “large” and a “small” cathode which, respectively, consisted of a 15-mm and 1.5-mm diameter CNT-coated circular area deposited on, respectively, a molybdenum and stainless steel substrate; see Fig. 1(b).

The experimental characterization of the cathodes was carried at the high-brightness electron beam source (HBESL) located at Fermilab.¹⁹ The facility incorporates a RF gun followed by a beam line instrumented with various beam diagnostics depicted in Fig. 2. The RF gun is a 1 + 1/2 cell resonant cavity operating on the $TM_{010,\pi}$ mode at $f_0 = 1.3$ GHz and is powered by a pulsed klystron capable of producing up to 2 MW of peak power. For the experiment reported in this letter, the klystron was operated at 1 Hz with a pulse duration of 30 μ s. The gun is nested in three magnetic lenses (referred to as “solenoids”) that nominally control the beam divergence and transverse emittance. The two cathodes described above were mounted on a standard cathode-plug holder and inserted in the RF gun. The available diagnostics along the downstream accelerator beam line includes a Faraday cup, several transverse-density monitors consisting of remotely insertable Cerium-doped Yttrium Aluminum Garnet (YAG:Ce) scintillators, and a set of capacitive electromagnetic pick-ups that can detect the transient electromagnetic field produced by the passing electron bunches. Several dipole magnets are used to deflect the beam and infer its mean momentum. Finally, the beam transverse emittance $\varepsilon_u \equiv \frac{1}{m_e c} [\langle u^2 \rangle \langle p_u^2 \rangle - \langle up_u \rangle^2]^{1/2}$ can be measured using a multi-slit method²⁰—here, (u, p_u) refers to the position-momentum coordinate along the horizontal ($u = x$) or vertical ($u = y$) degree of freedom, $\langle \cdot \rangle$ represents the statistical averaging over the beam phase space distribution, and m_e and c are the electron rest mass and the velocity of light. During the experiments reported below, the vacuum pressure was in the range of $[0.9, 1.2] \times 10^{-9}$ torr.

The field-emission process was first characterized by measuring the current dependence versus the applied macroscopic-field amplitude. The current inferred from the Faraday cup is time averaged, and its functional dependence on the time-dependent applied field is given by $\bar{I} = \frac{1}{\sqrt{2\pi}} \mathcal{A} a(\beta_e E)^{5/2} \exp\left(-\frac{b}{\beta_e E}\right)$,²¹ where the axial field is taken to be $\mathbf{E} = E \cos(2\pi f_0 t) \hat{n}$. The $\bar{I} - E$ curves display the expected exponential dependence of the current; see Figs. 3(a) and 3(c). Furthermore, when reported on a FN diagram [$1/E, \log(\bar{I}E^{-5/2})$], the data appear as lines and a linear-regression analysis provides information on the averaged enhancement factor and effective emission area as summarized in Table I for four of the cases studied. The settings of the three lenses were varied simultaneously and set to insure a zero magnetic field on the cathode surface and gave rise to an $\sim 10\%$ relative variation in produced beam current confirming that a significant fraction of the current is actually transversely captured and transported up to the location of the Faraday cup. We found the values of the enhancement factors to be independent of the applied magnetic field [Figs. 3(a) and 3(b)] and to be qualitatively similar for the two cathodes used during our experiments; see Figs. 3(c) and 3(d). It should be noted that the effective area \mathcal{A} is much smaller than expected for the small-area cathode. Assuming the same CNT density for both cathode, we would anticipate the effective emission area associated to the small cathode to be $(1.5/15)^2 = 10^{-2}$ while a factor $\sim [10^{-10} - 10^{-8}]$ is observed. A post-experiment inspection of the cathodes indicated some damages (dark spots) on the small cathode attributed to multipacting occurring due to the favorable secondary-emission yield of the stainless-steel substrate (strong multipacting emission was observed during operation of the small cathode). The small cathode also consistently degraded with time when operated at high field. The large cathode did not show any performance degradation despite being exposed to atmosphere for ~ 4 weeks between two subsequent tests.

The beam temporal structure of the electron beam formed by the large cathode was characterized using an electromagnetic pick-up located 30 cm from the cathode. The transient voltage induced by the bunches was detected by a capacitive coupler and recorded on a 12-Gs oscilloscope; a typical trace is displayed in Fig. 4(a). The detected signal can be factored as $V(t) = e(t) \sum_{n=1}^N \Lambda(t + n f_0^{-1})$, where $e(t)$ is the signal envelope and $\Lambda(t) \propto i(t)$ is the signal induced by one bunch. The amplitude of the fast-Fourier transform (FFT) of $V(t)$ provides the bunching factor $b(f)$ which is enhanced at harmonics of the bunch repetition frequency f_0

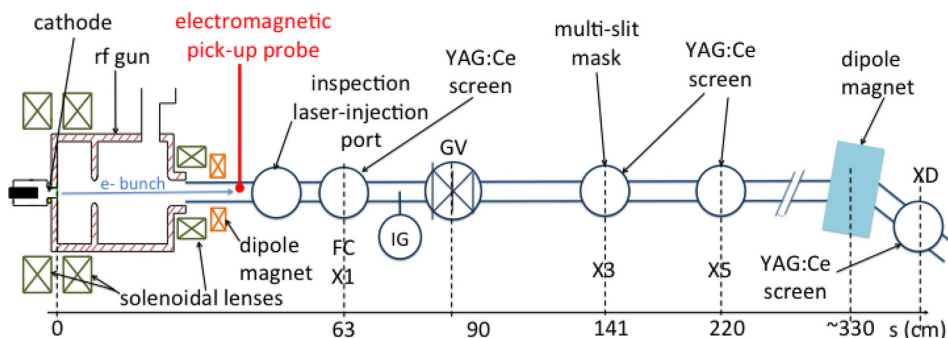


FIG. 2. Top-view schematics of the experimental setup of the HBESL facility. The “X’s” label indicates the location of diagnostics, “FC,” “IG,” and “GV,” respectively, stand for “faraday cup,” “ion gauge,” and vacuum “gate valve.” Only beam-line elements pertinent to the experiment are shown.

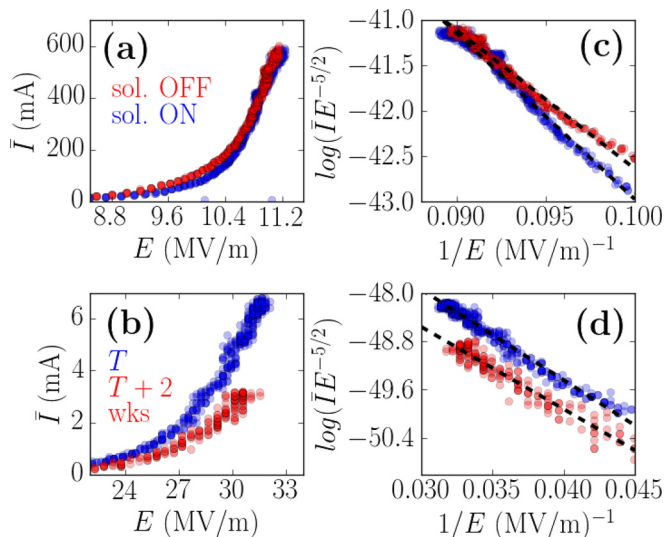


FIG. 3. Measured average current \bar{I} as a function of applied macroscopic field ((a) and (b)) and corresponding Fowler-Nordheim plots ((c) and (d)). The upper and lower rows, respectively, correspond to the large and small cathodes. The dashed lines in ((c) and (d)) represent linear polynomial fits. For plots (b) and (d), the blue and red symbols, respectively, correspond to data taken just after installation of the small cathode and 2 weeks later.

as shown in Fig. 4(b). The relative amplitudes $b(f)/b(f_0)$ at harmonic frequencies $f = n f_0$ (with $n \geq 2$) provide an upper bound for the bunch duration. Analysis of the data presented in Fig. 4(b), assuming the electron bunch follows a Gaussian temporal distribution, gives an rms bunch duration of $\sigma_t \simeq 67 \pm 25$ ps at an applied field $E \in [5, 12]$ MV/m. The electron-bunch duration is expected to scale as $\sigma_t \propto \sqrt{E}$ (Ref. 9) at the cathode. The bunch length increase with E_0 is supported by the observed increase of the $b(2f_0)/b(f_0)$ [see Fig. 4(c)], but due to the limited resolution of our pulse-length-measurement technique and the complicated dynamics in the RF gun, the functional dependence $\sigma_t(E)$ could not be characterized. In spite of these limitations, the measured pulse duration agrees reasonably well with particle-in-cell simulations performed with the Warp framework²² which includes a self-consistent field-emission model;²³ see Figs. 4(b) and 4(d). The FE parameters used in the simulations are the one reported for the large cathode (solenoid off) in Table I.

An important figure of merit of the field-emitted beam is its transverse emittance. The horizontal emittance of the full

TABLE I. Inferred enhancement factor β_e and effective emission area \mathcal{A} for the four operating cases considered in the text. The values are written as $A_{-y}^{+u} \pm w$, where A is obtained for a nominal work function value $\Phi = 4.9$ eV while the upper and lower uncertainties u and v are, respectively, evaluated for $\Phi = 5.4$ and 4.5 eV. The error bar w is propagated from the uncertainty on the linear regression.

Configuration	β_e	$\mathcal{A} \times 10^{16}$ (m ²)
Small cath., B field off	$468.1^{+73.4}_{-69.8} \pm 4.7$	$5.15^{+0.15}_{-0.22} \pm 0.10$
Small cath., B field off ^a	$504.6^{+79.2}_{-75.2} \pm 5.1$	$1.57^{+0.05}_{-0.07} \pm 0.03$
	β_e	$\mathcal{A} \times 10^8$ (m ²)
Large cath., B field off	$395.3^{+62.0}_{-58.9} \pm 4.0$	$10.18^{+0.29}_{-0.44} \pm 8.98$
Large cath., B field on	$468.1^{+73.4}_{-69.8} \pm 4.7$	$0.56^{+0.02}_{-0.02} \pm 0.21$

^aData taken 2 weeks later than data on previous line.

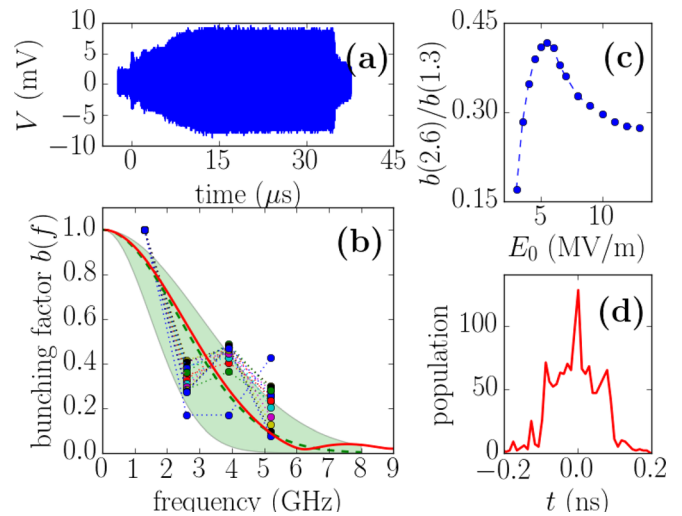


FIG. 4. Voltage detected from the electromagnetic pickup (a), corresponding bunching factor (b) and evolution of the bunching factor evaluated at $f = 2.6$ GHz as function of E_0 (c). In (b), the data points are FFTs of different traces obtained for different values of E_0 , the dash line represents a fit considering to a Gaussian bunch distribution (the shaded green area accounts for the uncertainties in the fit), and the solid thick line corresponds to the simulated bunch distribution using the Warp program shown in (d).

bunch train was characterized for the small cathode. The multislit mask located a position X3 was inserted, and the transmitted beamlets were observed at location X5. A measurement of the beamlet root-mean-square (rms) size at X5 provides information on the beam intrinsic divergence σ'_u at X3. Together with a measurement of the rms transverse beam size σ_u at X3, the divergence yield the value of the transverse normalized emittance as $\varepsilon_u = \beta \gamma \sigma'_u \sigma_u$, where $u \in [x, y]$ refers to one of the transverse degrees of freedom and $\beta \equiv (1 - \gamma^{-2})^{1/2}$ where γ is the relativistic Lorentz factor. An example of measurement with reconstructed phase space appears in Fig. 5. The measurement indicates a transverse horizontal emittance of $\varepsilon_x = 2.64 \pm 0.8 \mu\text{m}$ for the small

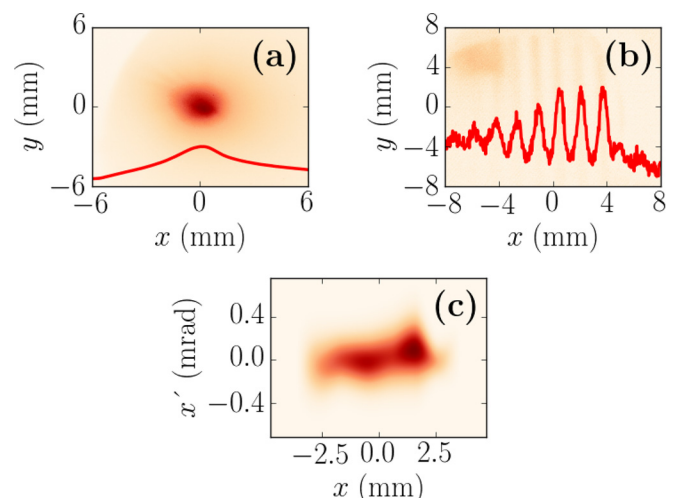


FIG. 5. Emittance measurement snapshots showing the beam transverse distribution at X3 (a), the transverse distribution of the beamlets transmitted through the multislit mask observed at X5 (b) with associated horizontal projections (red traces). Image (c) shows the reconstructed horizontal ($x, x' \equiv p_x/p_z$) trace spaces at the location of X3 from processing of images (a) and (b). These measurements were performed for the small cathode.

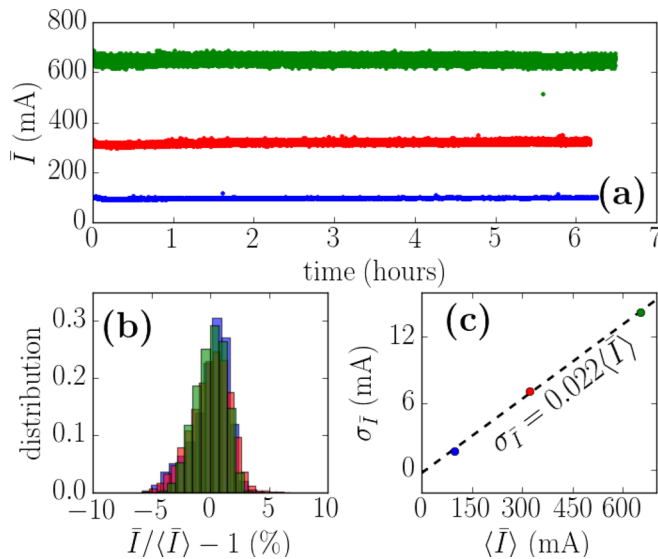


FIG. 6. Current evolution over a >6-h period (a) for 100 (blue), 300 (red), and 650 mA (green) with corresponding histograms (b) and rms fluctuations (c).

cathode. Measurements for the large cathode were compromised by the large energy spread.

Finally, the stability of a high-current electron source is crucial for some applications. We consequently tested the current stability for a few hours and confirmed that the cathodes under test were able to sustain the production of high-average currents with very low jitter; see Fig. 6(a). A statistical analysis also indicates that typical relative rms fluctuation of $\sigma_{\bar{I}} \equiv \langle \bar{I}^2 \rangle^{1/2} / \langle \bar{I} \rangle \simeq 2\%$ was achieved over six-hour periods and independently of the mean operating current $\langle \bar{I} \rangle$; see Figs. 6(b) and 6(c).

In summary, we have demonstrated the operation of a CNT cathode in the pulsed regime and produced bunch trains with operating average current up to $\bar{I} = 0.65$ A and duration of $\sigma_t \simeq 70$ ps, implying a charge per bunch $Q \simeq \bar{I}/f_0 \simeq 0.50$ nC corresponding to a single-bunch peak current $\hat{I} = Q/(\sqrt{2\pi}\sigma_t) \simeq 3$ A. The explored cold-cathode technology coupled with a superconducting resonator could lead to the development of high-average current quasi-continuous-wave electron sources. The main challenge toward such an endeavor remains the temporal control of the emission process as electrons field-emitted at unfavorable times are most likely to hit the resonator wall. Such collisions could result in secondary electron emissions and possible multipacting (as observed in some of our experiments) or could ultimately result in a superconducting quench of the cavity. Therefore, the development of gating schemes aimed at shortening the electron-bunch durations and preventing the back-propagation of electrons is crucial. A dual-frequency gun²⁴ supporting a fundamental and harmonic frequencies could effectively gate the emission of the CNT cathode to the proper phase of the accelerating RF wave. Since the CNT cathodes have a distinct threshold voltage, unlike thermionic cathodes, the bunch duration could be made much shorter, eliminating the need for a bunching structure before injection

into a subsequent accelerator. In such a scenario, it should be possible to reach ~ 10 -ps bunch durations.

We are grateful to D. P. Grote and J.-L. Vay for their help with Warp, to B. Chase, P. Prieto, E. Lopez, J. Santucci, and R. Kellett for technical support and to E. Harms, S. Nagaitsev, and V. Shiltsev for support. This work was funded via U.S. Department of Energy (DOE) Contract DE-SC0004459 with Radiabeam Technologies, LLC. Fermilab is operated by the Fermi Research Alliance, LLC. for the DOE under Contract DE-AC02-07CH11359.

¹I. Milne, K. B. K. Teo, E. Minoux, O. Groening, L. Gangloff, L. Hudanski, J.-P. Schnell, D. Dieumegard, F. Peauger, I. Y. Y. Bu, M. S. Bell, P. Legagneux, G. Hasko, and G. A. J. Amarutunga, *J. Vac. Sci. Technol., B* **24**, 345 (2006).

²E. W. Müller, *Z. Phys.* **131**, 136 (1951).

³C. A. Brau, *Nucl. Instrum. Methods Phys. Res., A* **393**, 426 (1997).

⁴R. H. Fowler and L. Nordheim, *Proc. R. Soc. London. Ser. A* **119**, 173–181 (1928).

⁵E. Minoux, O. Groening, K. B. K. Teo, S. H. Dalal, L. Gangloff, J.-P. Schnell, L. Hudanski, I. Y. Y. Bu, P. Vincent, P. Legagneux, G. A. J. Amarutunga, and W. I. Milne, *Nano Lett.* **5**(11), 2135 (2005).

⁶P. Hommelhoff, Y. Sortais, A. Aghajani-Talesh, and M. A. Kasevich, *Phys. Rev. Lett.* **96**, 077401 (2006).

⁷F. M. Charbonner, J. P. Barbour, L. F. Garrett, and W. P. Dyke, *Proc. IEEE* **51**, 991 (1963).

⁸K. B. K. Teo, E. Minoux, L. Hudanski, F. Peauger, J.-P. Schnell, L. Gangloff, P. Legagneux, D. Dieumegard, G. A. J. Amarutunga, and W. I. Milne, *Nature* **437**, 968 (2005).

⁹P. Piot, C. A. Brau, B. K. Choi, B. Blomberg, W. E. Gabella, B. Ivanov, J. Jarvis, M. H. Mendenhall, D. Mihalcea, H. Panuganti, P. Prieto, and J. Reid, *Appl. Phys. Lett.* **104**, 263504 (2014).

¹⁰S. V. Baryshev, S. Antipov, J. Shao, C. Jing, K. J. Prez Quintero, J. Qiu, W. Liu, W. Gai, A. D. Kanareykin, and A. V. Sumant, *Appl. Phys. Lett.* **105**, 203505 (2014).

¹¹W. Zhu, C. Bower, O. Zhou, G. Kochanski, and S. Jin, *Appl. Phys. Lett.* **75**, 873 (1999).

¹²G. N. Fursey, *Field Emission in Vacuum Micro-electronics* (Kluwer Academic/Plenum Publishers, New York, 2005), p. 138.

¹³M. Kumar and Y. Ando, *J. Nanosci. Nanotechnol.* **10**, 3739 (2010).

¹⁴*Electrophoretic Deposition of Nanomaterials*, edited by J. H. Dickerson and A. Boccaccini (Springer-Verlag, New York, USA, 2012).

¹⁵G. R. Neil, C. L. Bohn, S. V. Benson, G. Biallas, D. Douglas, H. F. Dylla, R. Evans, J. Fugitt, A. Grippo, J. Gubeli, R. Hill, K. Jordan, G. A. Krafft, R. Li, L. Meringa, P. Piot, J. Preble, M. Shinn, T. Siggins, R. Walker, and B. Yunn, *Phys. Rev. Lett.* **84**, 5238 (2000).

¹⁶G. I. Budker, *Sov. At. Energy* **22**(5), 438 (1967).

¹⁷M. Cleland and L. Parks, *Nucl. Instrum. Methods Phys. Res., B* **208**, 74 (2003).

¹⁸J. Hartzell, R. B. Agustsson, S. Boucher, L. Faillace, A. Y. Murokh, A. V. Smirnov, W. A. Hubbard, and C. Regan, in *Proceedings of the North-American Particle Accelerator Conference (NAPAC'13)*, Pasadena, CA USA, edited by S. Gourlay (2013), p. 394.

¹⁹J.-P. Carneiro, N. Barov, H. Edwards, M. Fitch, W. Hartung, K. Floettmann, S. Schreiber, and M. Ferrario, *Phys. Rev. ST Accel. Beams* **8**, 040101 (2005).

²⁰C. Lejeune and J. Aubert, “Emittance and brightness: Definitions and measurements,” in *Applied Charged Particle Optics, Part A*, edited by A. Septier (Academic Press, New York, 1980), p. 159.

²¹J. W. Wang and G. A. Loew, in *Proceedings of the Joint Us-Cern-Japan International School on Frontiers in Accelerator Technology, Hayama, Kanagawa, Japan, 9–18 Sep 1996*, edited by S. I. Kurokawa, M. Month, and S. Turner (1997), p. 768.

²²J. L. Vay, D. P. Grote, R. H. Cohen, and A. Friedman, *Comput. Sci. Disc.* **5**, 014019 (2012).

²³A. Seymour, D. Grote, D. Mihalcea, P. Piot, and J.-L. Vay, “Beam dynamics simulations of optically-enhanced field emission from structured cathodes,” Fermilab Report No. FERMILAB-CONF-14-363-APC (2014).

²⁴J. W. Lewellen and J. Noonan, *Phys. Rev. ST Accel. Beams* **8**, 033502 (2005).